Simulations of Crazing in Polymer Glasses: Effect of Chain Length and Surface Tension

A. R. C. Baljon

Department of Physics, San Diego University, San Diego, California 92182-1233

Mark O. Robbins*

Department of Physics and Astronomy, Johns Hopkins University, Baltimore, Maryland 21218

Received July 18, 2000; Revised Manuscript Received November 29, 2000

ABSTRACT: Craze formation determines the effective strength of many structural polymers and glassy polymer adhesives. We use molecular dynamics simulations to study the evolution of craze formation in glassy polymers as the number of monomers per chain N increases. When N is less than the entanglement length N_e, the polymer cavitates and then fails along a simple fracture plane. As N becomes greater than N_e, the mode of failure changes, and the entire volume deforms into a craze. As in experiment, crazing occurs at a constant plateau stress S and expands the volume of the polymer by a fixed extension ratio λ.

I. Introduction

The force at which a glassy polymer breaks is proportional to its toughness G, the work needed to propagate a crack through a unit surface area.[1,2] In a brittle material, G is nearly equal to the thermodynamic lower bound provided by the interfacial free energy 2γ of the crack surfaces. To be useful as structural materials or adhesives, polymers must have toughnesses that are 3−5 orders of magnitude larger than 2γ.

Experiments on glassy polymers show that that the excess work $G - 2\gamma$ goes into the formation of a craze near the crack tip (Figure 1).[3−6] Plastic deformation within the craze aligns the polymers into fibrils that merge and split to form an intricate network. An improved microscopic understanding of how these complex structures form may provide clues for making stronger adhesives. It may also improve our understanding of polymer entanglement, since crazes only form in un-cross-linked polymers when they exceed the entanglement molecular weight.

Previous theories of craze thickening have generally been based on macroscopic continuum equations.[3,4,7,8] While these theories are successful in reproducing some aspects of experiments, it is not clear that continuum concepts are valid for fibril diameters D that are of order 10 nm. It is also not clear that equilibrium quantities like surface tensions are relevant for the very nonequilibrium process of craze formation. Such issues are readily addressed through simulations, but most previous studies of polymer failure have not considered entangled chains or not been large enough to observe a fully developed craze structure.[9−14] One exception is recent work by Stevens,[15] but these studies consider highly cross-linked polymers where entanglement is irrelevant.

In this paper we present molecular dynamics simulations of craze formation using a simple model potential. These simulations reproduce many features of experiments[3,4,16] and indicate difficulties with existing theoretical models. We find that polymers must be longer than the entanglement length N_e before a stable craze can form but that there is little dependence on chain length for longer polymers. As in experiment, the craze thickens at a constant plateau stress S. This value represents the stress to convert material at the boundary of the craze into a craze network (Figure 1). In the process, the volume of the polymer increases by a fixed extension ratio λ. Simple models for S and λ are tested by varying the interaction potential.

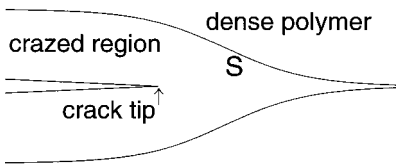

Figure 1. Sketch of a crack tip moving through a glassy polymer. A craze network surrounds the crack tip. Experiments show that it forms by pulling material from dense polymer at the outer boundary of the craze. In the process, the volume increases by the extension ratio λ. There is a constant plateau stress S along the outer boundary of the craze. The craze thickens as the crack tip approaches and can become many micrometers wide.

The following section describes the model used to describe glassy polymer adhesives and the geometry used to induce failure. Section IIIA compares the toughness and failure mechanisms of different length polymers. Then the effect of reducing surface tension on S and λ is explored. Section IIID discusses the possibility of chain scission, and section IV presents a summary and conclusions.

II. Computational Methodology

A. Polymer Model. Our goal is to use the simplest model that captures the general features of craze formation. Thus, the polymers are described with a bead−spring model that has been shown to yield realistic dynamics for polymer melts.[17,18] Each polymer contains N spherical beads of mass m. All beads interact through a truncated 6−12 Lennard-Jones potential. The

10.1021/ma0012393 CCC: $20.00
Published on Web 05/05/2001

potential is zero if the separation r between two beads exceeds a cutoff radius r_c. For $r < r_c$,

$$V_{LJ}(r) = 4\epsilon[(\sigma/r)^{12} - (\sigma/r)^6] - 4\epsilon[(\sigma/r_c)^{12} - (\sigma/r_c)^6] \quad (2.1)$$

where the second term shifts the potential to zero at r_c, and ϵ and σ are characteristic energy and length scales, respectively. These and the characteristic time, $\tau_{LJ} \equiv (m\sigma^2/\epsilon)^{1/2}$, are used to make all of our calculated quantities dimensionless.

Nearest-neighbor beads along a polymer are coupled by an additional potential

$$V_{CH}(r) = -\frac{1}{2}kR_0^2 \ln[1 - (r/R_0)^2] \quad (2.2)$$

where $R_0 = 1.5\sigma$ and $k = 30\epsilon/\sigma^2$. This potential ensures that polymers cannot pass through each other in equilibrium simulations.[17] We have monitored the maximum separation of neighboring beads to make sure that chain crossing does not happen under the stresses produced in our nonequilibrium simulations. The maximum separation also gives the maximum stress in any bond. One of the artificial features of V_{CH} is that the polymers cannot undergo scission. However, as discussed in section IIID, the maximum stresses we observe are too small to produce significant scission in more realistic models of polymers.

Kremer and Grest have discussed the mapping of this bead−spring model to real polymers.[17] On the basis of a comparison of calculated and experimental entanglement lengths, they found that each bead corresponds to $^1/_2$−5 repeat units. This variation reflects differences in the flexibility and length of repeat units. The corresponding values of σ range from 0.5 to 1.3 nm. The energy ϵ represents the van der Waals interaction between two polymer segments of this length, and Kremer and Grest quote a range from 2.5 to 4 kJ/mol (25 to 40 meV) for different polymers.

B. Geometry. It is not possible to simulate the entire region illustrated in Figure 1 on current computers. We focus on a simpler geometry where walls apply a pure tensile stress to a glassy polymer. This allows us to study the initial nucleation of cavities that occurs before the craze develops and the subsequent thickening of the craze by pulling material from the undeformed regions at its outer boundary. Most of the toughness of polymers comes from the craze thickening process.[6]

The polymer is confined between two rigid walls containing discrete atoms. The lattice sites of each wall form two (111) layers of an fcc crystal. Each atom is tied to its lattice site by a spring whose stiffness, κ, is adjusted to make sure that thermal displacements are small compared to the Lindemann criterion for melting.[19] We use $\kappa = 360\epsilon\sigma^{-2}$during rupture of the films at $T = 0.3\epsilon/k_B$.

Wall atoms interact with beads through a Lennard-Jones potential with the same length scale and cutoff as the bead/bead interaction. The energy scale ϵ_w is varied from ϵ to 3ϵ. For $\epsilon_w \geq \epsilon$ failure initiates within the polymer rather than at the polymer/wall interface, in agreement with previous work on shorter chains.[11] As discussed below, the wall/bead interactions have little influence on the deformation of the polymer until the very final stages of failure when a craze occupies the entire volume.

The walls are parallel to the $x-y$ plane, and periodic boundary conditions are applied in these directions. These periodic boundary conditions prevent lateral stresses from relaxing completely. However, the lateral stresses in the crazed region are very small. The polymer is subjected to a pure tensile strain by fixing the bottom wall and moving the top wall away from it at a velocity v along the z axis. To avoid creating shock waves, the wall is accelerated smoothly to v over at least $50\tau_{LJ}$. This corresponds to a displacement of order σ, and the stress remains below the yield stress during this acceleration. Experiments on glassy polymers show little change in toughness with velocity (e.g., a factor of 2 over 8 decades in velocity for PMMA[5]), and our previous simulations of glassy polymers also showed little change with v up to the velocities used here: $0.03-0.06\sigma/\tau_{LJ}$.[9] Using the maximum possible velocity lowers the computation time and allows us to access larger systems. Tests of velocity dependence are described in section III.

The equations of motion for the beads and wall atoms are integrated using the fifth-order Gear predictor−corrector algorithm.[20] The time step dt is $0.005\tau_{LJ}$ for runs with 24 576 beads and $0.0075\tau_{LJ}$ for larger systems. A linked-cell algorithm and Verlet list is used to obtain linear scaling of compute time with system size.[20] The code is optimized for DEC Alpha workstations. On a 400 MHz ev5 processor a single time step for a 24 576-bead system takes about half a second. Our longest runs with 262 144 beads for 10^6 time steps take about 2 months.

Constant temperature is maintained by adding a Langevin noise term and damping to the equations of motion of wall atoms.[21] As the thickness of the film increases, the transport of heat to the walls can become too slow to maintain a constant temperature in the center of the polymer. This can produce velocity-dependent changes in failure mechanisms that merely reflect the temperature change. The temperature rise can be eliminated by lowering the velocity as the thickness increases, but the required simulation time then increases as the fourth power of the film thickness.

To avoid this problem, we coupled a weak thermostat to the x and y components of the equations of motion of all beads in some simulations with thick films. This direct cooling is artificial, but we found that runs using it for our largest systems gave nearly the same results as simulations with lower velocities, and that the results were not sensitive to the strength of the thermostat. Equivalent results were also obtained from simulations with a Verlet integration scheme[20] and a Nose-Hoover thermostat.[22]

C. Equilibration. Care must be taken in creating initial states of the polymer because of the long diffusion times for chains that exceed the entanglement length. We use the technique of Kremer and Grest,[17] with a modification to include the bounding walls.

The initial configuration of each polymer is a random walk. The position of the end of the chain is chosen at random. Successive beads are then added, separated by a distance equal to the equilibrium bond length. The only constraint on the direction of subsequent bonds is that next-nearest neighbors are not allowed to overlap. More distant beads may overlap. The equilibrium bond length, 0.96σ, and minimum distance between next-nearest neighbors, 1.0σ, were determined from runs with shorter polymers that equilibrate rapidly. Walls are included by rejecting new sites that are too close to

a wall atom (less than about 0.3σ) and choosing another position at random.

The resulting initial configurations have many overlapping beads. To gradually impose an excluded-volume constraint, a simulation is done with a repulsive cosine potential between bead centers.[17] The magnitude of the cosine potential is gradually increased over this run. The system can then be equilibrated further using the bead−spring potential described above.

For the results described below, we fix the walls at a separation that places the film under a small compression at $T = 0.3\epsilon/k_B$. The temperature is then raised to $1.3\epsilon/k_B$ to speed diffusion and gradually lowered back to $0.3\epsilon/k_B$.The equilibration time is greater than 10^5 time steps for the results presented here, but much shorter equilibrations give equivalent results. For runs with $r_c = 2.2\sigma$, the density in the regions away from the walls is $\rho = 1.05\sigma^{-3}$, and the initial compressive pressure p varies from nearly 0 to $0.3\epsilon\sigma^{-3}$. In runs with $r_c = 1.5\sigma$, the density is $\rho = 1.00\sigma^{-3}$, and p varied from $0.5\epsilon\sigma^{-3}$ to $0.9\epsilon\sigma^{-3}$. We checked that our results were not sensitive to much larger density changes of 1 or 2% that varied the initial pressure from a compression of $4\epsilon\sigma^{-3}$ to a tension of $-0.4\epsilon\sigma^{-3}$. The radius of gyration of the polymer chains scales as $R_g^2/(N-1) \equiv b^2/6 = 0.28(1)\sigma^2$ for all cases, implying that the effective segment length $b = 1.30(2)\sigma$.

The above equilibration scheme mimics setting of a thermal adhesive that is clamped at a fixed spacing and produces an isotropic initial state in the center of the film. We also tried to mimic an unclamped case by allowing the top wall to move up and down to maintain zero pressure as the temperature changed. However, we found that this created an anisotropic initial condition because the dimensions in the $x-y$ plane were fixed and only the height varied. As T decreased, the polymer contracted. The top wall moved in to relax the zz component of the stress tensor, but large local rearrangements in the polymer were needed to relax stresses in the $x-y$ plane. Once the temperature dropped below the glass transition, these local rearrangements were inhibited until the yield stress was exceeded. Thus, the final state had large anisotropic stresses and regions where plastic deformation had occurred. As a result, the yield stress was always lower than with the fixed wall equilibration, and other quantities were less reproducible.

D. Entanglement Length. Kremer and Grest[17] and Pütz et al.[18] have studied entanglement for a bead−spring model like that used here. They found that the crossover in diffusion gives an entanglement length of 30−35 beads, while the plateau modulus gives slightly more than twice this value. This discrepancy may reflect more complicated dynamics than current theoretical models predict[23] or merely a difference between prefactors that are not well determined in these models.[18]

Since experiments usually determine N_e from measurements of the plateau modulus, we will use the value Pütz et al.[18] obtained from this technique: $N_e = 74 \pm 9$. However, their simulations used different parameters than ours: $\rho = 0.85\epsilon^{-3}$, $T = 1.0\epsilon/k_B$, and a purely repulsive potential, $r_c = 2^{1/6}\sigma$. The latter choice is not physical for studies of adhesives, and we extend the cutoff into the attractive tail of the potential, using $r_c = 1.5\sigma$ or 2.2σ below.

Theory suggests that changing r_c and T does not affect N_e directly.[24] However, both change the equilibrium density of the polymer, which is expected to change N_e. To our knowledge their have been no simulations studying this effect. Experimental data on a set of polymers with different densities[24] supports a prediction that N_e scales as $(b^3\rho)^{-2}$. This would suggest that our N_e could be smaller than that of Pütz et al. by 30−35%, giving $N_e = 50 \pm 10$. However, the experimental data do not test changes in N_e with density for the same polymer, and experimentalists normally quote the entanglement length for the melt even though the glass has a lower density. In addition, it is not obvious whether the initial density or the density of the region that is in equilibrium with the craze is relevant.

For all of the above reasons the proper value of N_e is uncertain, but it is in the range between 40 and 80. We will examine chain lengths of 16, 32, 64, 128, and 256 that span from roughly $^1/_4N_e$ to $4N_e$.

III. Results

A. Chain Length Dependence of Stress and Failure Mode. We first examine changes in failure mode with chain length N in systems with 24 576 beads and $r_c = 2.2\sigma$. In each case the walls are 38.53σ by 33.37σ in the $x-y$ plane. The initial separation between the innermost layers of wall atoms is 18.8σ. This leads to a mean density in the center of the film of $1.05\sigma^{-3}$, which corresponds to a slightly compressed state of the film. The initial pressure on the wall varies from about 0 to $0.3\epsilon\sigma^{-3}$, depending on chain length and initial conditions. All runs are done with $\epsilon_w = 2\epsilon$ and $T = 0.3\epsilon/k_B$, which is below the glass transition temperature ($T_g \approx 0.5\epsilon/k_B$).[25]

After equilibration, the walls are separated at velocity $v = 0.03\sigma/\tau_{LJ}$. This velocity was chosen based on previous studies[9,10] of similar glassy films with $N = 16$. There the toughness changed only from $8.6\epsilon\sigma^{-2}$ to $9.3\epsilon\sigma^{-2}$ as v increased from $0.001\sigma/\tau_{LJ}$ to $0.03\sigma/\tau_{LJ}$. Further increases in velocity to $0.1\sigma/\tau_{LJ}$ and $0.3\sigma/\tau_{LJ}$ produced much larger increases in G.

Figure 2a shows the force needed to displace the top wall as a function of the distance moved for N between 16 and 256. The same force is exerted on the bottom wall, indicating that there is time for pressure fields to equilibrate throughout the system. For small displacements the polymer responds elastically: There is a linear increase in force with the wall displacement. The force continues to rise until it reaches a yield stress of about $3.5\epsilon\sigma^{-3}$ and then drops sharply. This initial peak and drop is independent of the chain length. Examination of the bead positions shows that one or more cavities nucleates at the peak. These initial cavities occur at random positions.[26] As the force drops, a failure plane evolves that is oriented perpendicular to the tensile stress. Cavities lying along the failure plane grow and merge, while other cavities shrink. This evolution is independent of N as long as the cavities remain small compared to both N and N_e.[11,12] However, the late stages of growth are very sensitive to the value of N.

For $N = 16$ and 32, the force decays rapidly to zero as the wall displacement increases. Figure 3 shows projections of the $N = 32$ system at four different stages of failure. As in our earlier studies[9,10,12] for $N = 16$, cavities grow and merge until there are only a few simple strands joining the surface along the failure plane. The chains in these strands then pull free of each other and collapse onto one of the surfaces. The total

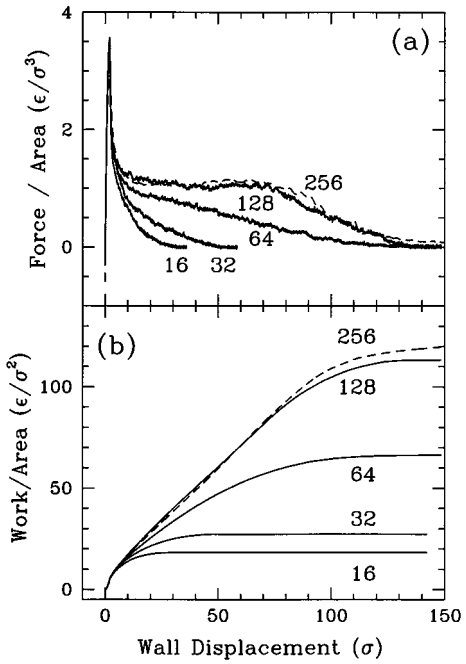

Figure 2. Variation with wall displacement of (a) stress needed to displace the top wall and (b) total work done for the indicated chain lengths in systems with 24 576 beads. The final value of the work gives the toughness G. For $N < 128$ the stress drops rapidly to zero, and the toughness is small. For $N = 128$ and 256 (dashed lines) a stress plateau develops. This leads to a linear rise in work with wall displacement. Analysis of Figures 3−7 shows that the linear increase in work is limited only by the system size, up to the largest scales accessible to us (∼200 nm).

toughness, given by the total integral of force vs distance, is shown in Figure 2b. For both $N = 16$ and 32 the toughness is quite small—only a factor of 6−9 above the lower bound provided by the change in equilibrium free energy ($2\gamma \approx 3\epsilon\sigma^{-2}$).[9] As N increases to 64, the tail in the force lengthens, and the tendrils connecting the surfaces become slightly more complicated, but the failure is still relatively simple (Figure 3).

The early evolution of films with $N = 128$, 192, and 256 is the same as for $N < N_e$: Cavities grow and merge within a plane, creating short fibrils. However, for $N > N_e$ the polymers in these fibrils are no longer able to pull free from each other. The evolution of the material in the original failure plane becomes arrested, presumably by entanglements. This initial "precrazed" region[16] becomes stronger than the surrounding, undeformed material. As the walls separate further, material at the edge of the craze is gradually deformed to become part of the craze. This thickening process continues until the whole volume of the polymer is deformed. The polymer then pulls off from one wall, indicating that crazing has made it stronger than the wall/polymer interface. As the craze spreads, there is a plateau in the stress, and the work done increases linearly with the wall displacement. The eventual failure at the wall limits the range of the plateau, and thus the total toughness, but G is still much larger than for $N = 64$. Stress curves for $N = 128$, 192, and 256 are nearly the same, within statistical fluctuations.

Test runs at $v = 0.01\sigma/\tau_{LJ}$ yielded almost the same stress/displacement curves and failure sequence. Increasing the velocity to $v = 0.06\sigma/\tau_{LJ}$ did not change the plateau stress but did lengthen the final tails in the stress curves. These tails occur after craze formation, when chains pull free from one wall, and higher velocities increase the dissipation during this process. Since we are interested in craze thickening rather than the final interfacial failure, we increased the velocity to $0.06\sigma/\tau_{LJ}$ for all the runs described below.

To show that the plateau in the stress (Figure 2) is limited by the amount of material rather than any intrinsic length of the entangled polymers, we show snapshots from a simulation in a much larger system (98 304 beads with $N = 256$) in Figure 4. A cavity forms near the top of the system and has nearly reached its final width by the first snapshot. As the walls move out further, the cavity extends vertically in both directions. As in experimental studies of craze thickening,[4,16] deformation is confined to narrow "active zones" at the interfaces between the dense polymer regions near the walls and the less dense craze. The final state consists of one or two main fibrils that are most clearly seen in the top panels. These bundles of highly aligned polymers are nearly parallel to the vertical axis along which strain is applied. A series of lateral "cross-tie" fibrils are generated that is most clearly seen in the bottom panels. Once formed, they retain their structure in subsequent panels. Animations generated from this and other simulations[26] are very consistent with the cold-drawing mechanism for craze thickening seen in experiments.[4,16] Fibrils form as polymers are pulled out of the boundary of the dense regions adjacent to the craze. The width of the active zone is discussed further below (Figure 8).

The process of craze thickening continues until the whole system is converted from the initial dense state to a network of voids and fibrils. Plots like Figure 2a show that the stress has a constant plateau value $S = 1.1(1)\epsilon\sigma^{-3}$ during the entire failure process. As a result, the work continues to rise linearly up to displacements of about 250σ before failure occurs at the wall. The final toughness is about $300\epsilon\sigma^{-2}$, roughly 100 times the change in equilibrium free energy.

Our unit of pressure, $\epsilon\sigma^{-3}$, corresponds roughly to 40 MPa, taking typical values[17] of $\epsilon = 3$ kJ/mol and $\sigma = 0.5$ nm. Thus, our calculated plateau stress is well within the range of experimental values for real polymers. For example, the experimentally measured plateau stress for polystyrene is 30−40 MPa at room temperature,[4] while the value for PMMA is about 70 MPa.[6] However, there is an uncertainty of at least a factor of 2 in our units due to the difficulties in mapping the bead spring model to real polymers and to variations between polymers. More quantitative comparisons to experiment are not possible without using realistic molecular potentials. However, we can test predicted trends in S and craze structure.

B. Effect of Surface Tension on Fibril Spacing. The structures shown in Figures 3 and 4 are reminiscent of real space images of experimental craze structures.[3,4,16] These structures are often modeled by the even simpler geometry sketched in Figure 5. Here the fibrils are assumed to be cylinders directed along the applied tension with diameter D and spacing D_0. Values of D and D_0 are usually obtained from a fit to X-ray or electron diffraction measurements.[4,27,28] However, detailed examination of these results, and of real space images, shows that there is a broad range of diameters and spacings and that the fibrils are tilted and interconnected.[4]

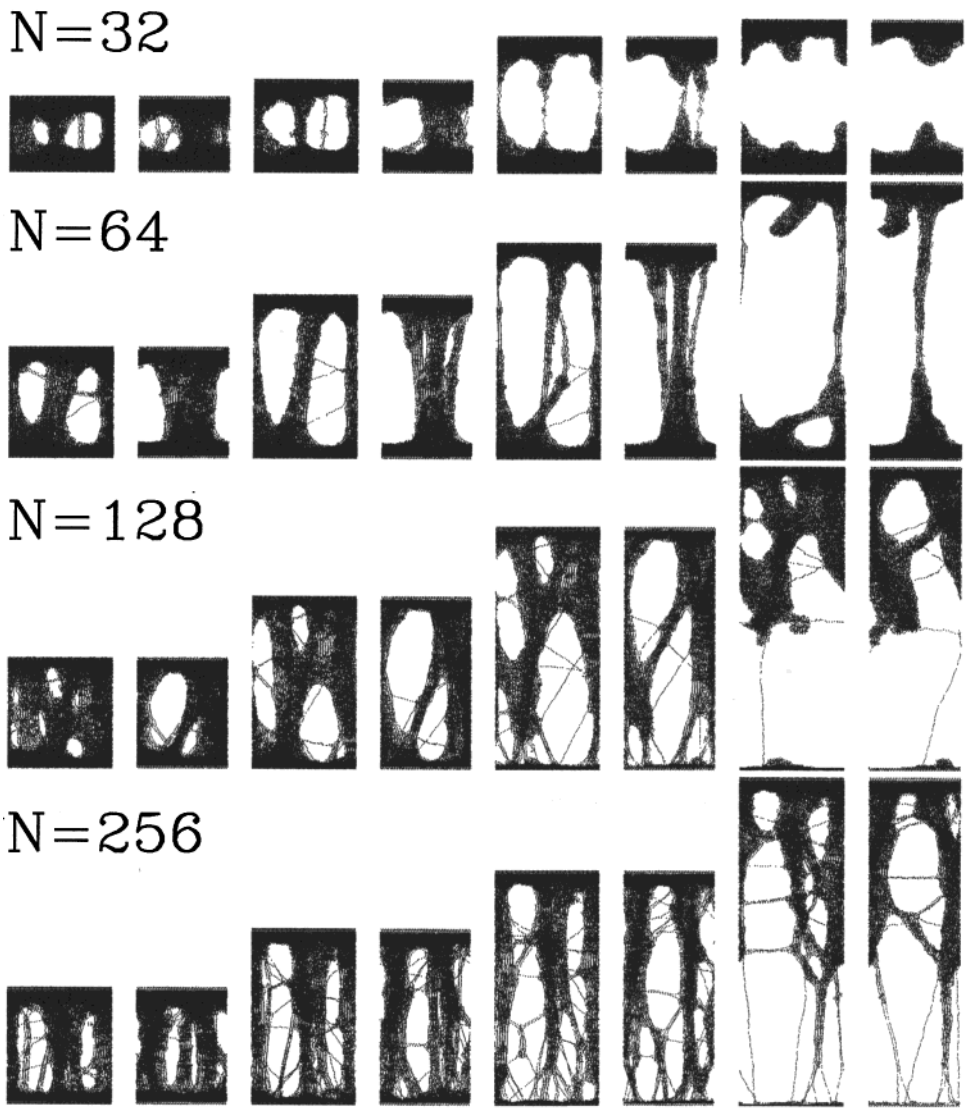

Figure 3. Snapshots during rupture in systems with 24 576 beads, $r_c = 2.2\sigma$, $\epsilon_w = 2\epsilon$, and the indicated chain lengths N. The top wall is displaced upward along the z axis at $v = 0.03\sigma/\tau_{LJ}$. Projections in the $x-z$ plane and $y-z$ plane are shown at four progressive stages of rupture (time increases from left to right). The time interval between projections increases with N because the total time to failure increases. Periodic boundary conditions are applied in the $x-y$ plane, with periods of 38.53σ and 33.37σ, respectively.

Theories of craze thickening have assumed that D and D_0 are determined by an interplay between an effective interfacial tension Γ_{eff} and viscous forces.[3,4,8] The models differ in the assumed relation between Γ_{eff} and the equilibrium interfacial tension γ of the polymer, and between stress and strain rate. Kramer and co-workers predict that decreasing the interfacial tension decreases both D and D_0, because the penalty for creating more surface area is reduced.[3,4] Krupenkin and Fredrickson[8] conclude that D is always of order the Euclidean distance between entanglements $l_e = bN_e^{1/2}$.

To test the above predictions for the effect of surface tension, we changed the cutoff r_c in our Lennard-Jones potential from 2.2σ to 1.5σ, which is near the first minimum in the pair correlation function of the bulk polymer. This removes much of the attractive tail in the potential and thus reduces the equilibrium surface tension from $1.6 \pm 0.2\epsilon\sigma^{-2}$ to $0.6 \pm 0.1\epsilon\sigma^{-2}$. However, the entanglement length is expected to remain nearly unchanged.[24]

Simulations with the same size system as Figure 4 show that the mean number of fibrils per periodic cell in the $x-y$ plane increases from about one to four when r_c decreases from 2.2σ to 1.5σ. Figure 6 shows results for an even larger system with 262 144 beads. The x and y dimensions were doubled to 77.06σ by 66.74σ, and the initial spacing between wall surfaces was 53.2σ. Cross sections show that the mean number of fibrils per cross section is about 15, an increase over the smaller system by roughly the factor of 4 increase in area. This fibril density corresponds to a mean fibril spacing $D_0 \sim 20\sigma$. There is a broad distribution of fibril sizes with a mean diameter of about 7σ and a root-mean-square (rms) diameter of 11σ. These values of D_0 and D are roughly half the values for $r_c = 2.2\sigma$, although our statistics for the latter case are too small to get a precise ratio. Kramer et al.[3,4] predict D and D_0 should scale as $\gamma^{1/2}$. This would imply a change in D by a factor of 1.6 ± 0.2, which is roughly consistent with our observations. Our results are not consistent with Krupenkin and Fredrickson's prediction that D and D_0 are independent of surface tension.[8] However, their model correctly predicts the fibril spacing in many experimental systems, and inserting $N_e = 64$ and our values for b and λ (see below) into their expressions yields values of $D = 13\sigma$ and $D_0 = 23\sigma$ that are comparable to our results

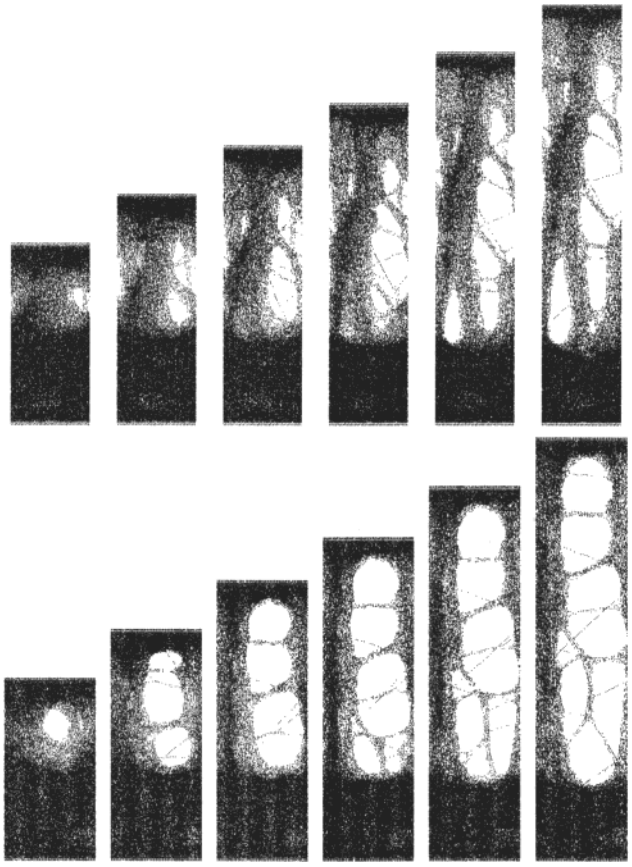

Figure 4. Snapshots during rupture in a system with 98 304 beads, $N = 256$, $\epsilon_w = 2.5\epsilon$, and $r_c = 2.2\sigma$. Projections in the $x-z$ (bottom) and $y-z$ (top) planes are shown at seven progressive stages of rupture (time increases from left to right). From the top panels, one sees the evolution of one or two main fibrils running vertically along the strain direction. The bottom panels show the generation of a series of cross-tie fibrils. Once a region has been converted to a craze network, there is little apparent change in its geometry. Periodic boundary conditions are applied in the $x-y$ plane, with periods of 38.53σ and 33.37σ. Although the fibril spacing is comparable to the system size in this figure, larger simulations give a similar spacing.

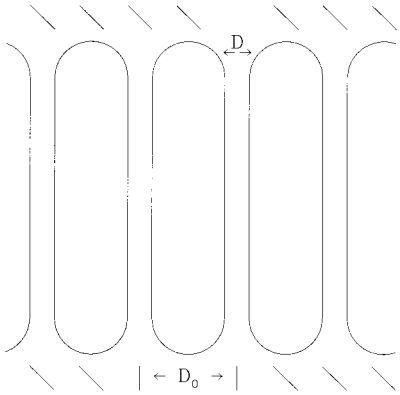

Figure 5. Simple model of the structure of crazes. Fibrils are cylinders of diameter D directed vertically along the applied tension and are spaced by D_0. The plateau stress is often assumed to equal the Laplace pressure from the curved interfaces at the boundary between fibrils and undeformed material.[3,4,7,8]

for $r_c = 1.5\sigma$. It may be that part of the discrepancy between our results and their model is due to a decrease in T_g with decreasing r_c or to the fact that lateral stresses cannot fully relax in our simulation geometry.[26] These effects are under study.

While the larger size of the system in Figure 6 leads to a much more complex structure than in Figure 4, a similar process is occurring. Several cavities nucleate, and the ones lying in a failure plane grow and merge to form a "precraze". The craze then thickens by pulling fibrils from the surrounding polymer. Deformation is confined to a thin active zone between the dense and crazed regions. Once polymers are pulled out from the dense region into fibrils, they retain this structure in subsequent snapshots.

Figure 7 shows a series of stress/displacement plots for different polymer lengths with $r_c = 1.5\sigma$ and 98 304 beads. These plots show the same trends with N that were seen in Figure 2. The initial stress peak and decay is nearly independent of N, but the late stages of failure are very different for $N < N_e$ than for $N > N_e$. For short polymers ($N < 64$) the stress falls rapidly to zero, while for $N \geq 128$ the stress fluctuates about a plateau value. The fluctuations can be correlated to stages in the formation and growth of individual fibrils. Studies with 262 144- and 884 736-bead systems show that increasing system size reduces the fluctuations about the plateau stress without shifting its average value.

The value of the plateau stress S decreases from $1.1(1)\epsilon\sigma^{-3}$ to $0.48(3)\epsilon\sigma^{-3}$ as r_c decreases from 2.2σ to 1.5σ. Macroscopic models of craze thickening[3,4,7,8] equate the plateau stress to the Laplace pressure at the intersection between fibrils and the undistorted material (Figure 5). This implies $S \propto \gamma/D_0$, since the radius of curvature of the interface is of order D_0. Changing r_c from 2.2 to 1.5 reduces γ by about a factor of 2.5 and D_0 by about a factor of 2. Thus, the Laplace pressure should drop, but not by as large a factor as observed. In addition, the absolute values of S are larger than we would expect from the observed radii of curvature of the interface. It has been argued that the effective surface tension Γ_{eff} may be higher than the equilibrium γ due to chain scission;[4,8] however, scission is neither observed nor likely for our system (section IIID). A more likely source for the enhanced value of S is that the Laplace pressure only represents the stress carried along the interface, and stress can also be transmitted along the backbones of the polymers that extend from the fibrils into the uncrazed material. Future studies of the three-dimensional stress distribution near the craze interface will be able to resolve this issue.

A more subtle difference between Figures 2 and 7 is seen when the results for N near N_e are compared. For $r_c = 2.2\sigma$, simulations with 98 304 beads at $N = 128$ do not show as clear a plateau stress as simulations with $N = 192$ or 256. The real space structures also indicate that $N = 128$ systems form single strands between the walls at late times. When r_c is reduced to 1.5σ, runs with $N = 128$ exhibit clear stress plateaus, although the value is slightly lower than for $N = 192$ and 256 and appears to decrease with decreasing velocity ($\sim$10% as v decreases from $0.06\sigma/\tau_{LJ}$ to $0.02\sigma/\tau_{LJ}$). Runs with $N = 64$ also exhibit a larger tail for $r_c = 1.5\sigma$ than for $r_c = 2.2\sigma$. These results indicate that the length needed to obtain a stable craze is shifted slightly with r_c. This may be because the smaller stresses for $r_c = 1.5\sigma$ are less likely to disentangle chains.

C. The Extension Ratio. As noted in the Introduction, experimental studies of craze growth find that crazing increases the volume occupied by the polymer by a well-defined factor called the extension ratio λ. Different values of λ are measured for different poly-

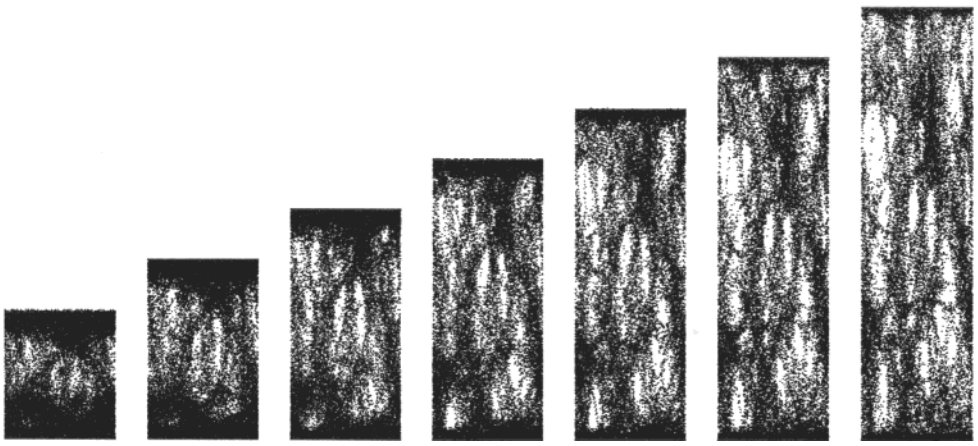

Figure 6. Monomer positions during rupture in a system with 262 144 beads, $N = 256$, $r_c = 1.5\sigma$, and $\epsilon_w = 3\epsilon$. Projections onto the $x-z$ plane are shown at seven progressive stages of rupture (time increases from left to right). Note that the first fibrils to form do not evolve as time progresses. Instead, new fibrils are formed from the adjacent material as the active zone moves through the dense polymer regions that bound the craze. Decreasing r_c produces much finer structure than in Figure 4 where the periods in the x and y directions are half as large.

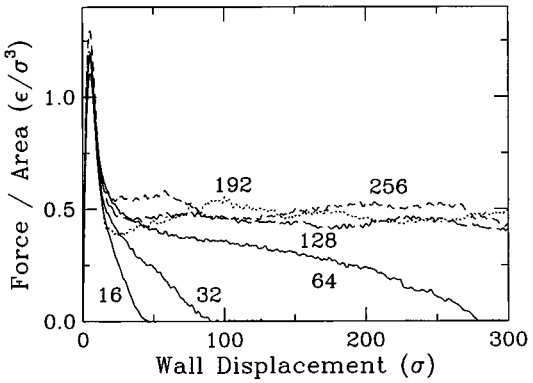

Figure 7. Stress needed to displace the top wall as a function of wall displacement for the indicated chain lengths in systems with 98 304 beads and $r_c = 1.5\sigma$. The trends with N are similar to those in Figure 2. For $N < 64$ the stress drops rapidly to zero, while for $N > 64$ the curves show a long stress plateau. The plateau stresses for $N = 192$ and 256 are the same within statistical fluctuations, but the plateau stress for $N = 128$ is slightly smaller. Decreasing r_c lowers both the peak stress needed to nucleate cavities and the plateau stress.

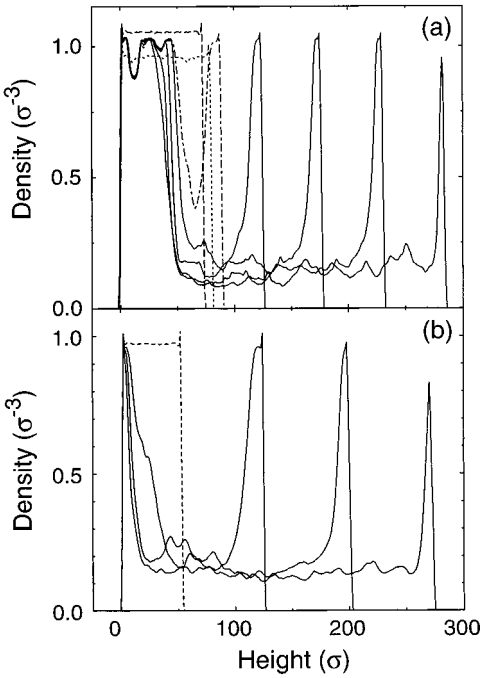

Figure 8. Density as a function of height above the bottom wall during different stages of rupture for (a) $r_c = 2.2\sigma$ and 98 304 beads and (b) $r_c = 1.5\sigma$ and 262 144 beads. In both cases, $N = 256$ and the dashed line shows the initial density. The first three solid curves correspond to the times of the second, fourth, and sixth snapshots in Figures 4 and 6. The final curve in each panel shows a decrease in the density near the top wall that indicates interfacial failure will occur. The distance ($\sim 10\sigma$) over which the density changes from the initial value to that of the craze gives an indication of the width of the active zone.

mers. However, λ is relatively insensitive to factors that change the fibril spacing for a given polymer.[4] Kramer has proposed a simple model for λ that assumes entanglements act like permanent chemical cross-links between polymers that are spaced by N_e along the backbone.[3,4] In the initial unstressed state, the polymer follows a random walk. The rms Euclidean distance between entanglements is $b(N_e - 1)^{1/2}$ where $b = 1.30(2)\sigma$ for our systems. After crazing, the maximum Euclidean distance between entanglements is $(N_e - 1)d_{nn}$, where $d_{nn} = 0.96\sigma$ is the mean distance between nearest-neighbor beads along the chain. Taking the ratio of these distances gives an approximate upper bound on λ

$$\lambda_{max} \equiv (N_e - 1)^{1/2}(d_{nn}/b) \qquad (3.1)$$

Using the value of $N_e = 74 \pm 9$ from Pütz et al.[18] in the above equation gives $\lambda_{max} = 6.4 \pm 0.4$. If N_e needs to be corrected to account for the different density used in our simulations (section IID), then λ_{max} would fall to 5.5 ± 0.5.

The value of λ is normally measured in experiment by comparing absorption through crazed and uncrazed regions of polymer films in transmission electron microscope images.[4] Since the film thickness is nearly unchanged, the amount of absorption is proportional to the density. The extension ratio is given by the ratio of the density in the uncrazed region to that in the craze.

Figure 8a shows the density as a function of height z above the bottom wall at several different times for the system of Figure 4 where $r_c = 2.2\sigma$. In the initial state (dashed line), the density in the center of the system is constant.[29] As the walls begin to move apart, the stress

rises, and the density decreases uniformly throughout the system (dotted line). Shortly after the peak stress, a layer of cavities has formed, producing a narrow dip in the density near $z = 70\sigma$ (dash−dotted line). As the cavities spread within the plane, the dip in density widens and the minimum density drops. If N was less than N_e, the density would continue to drop to zero, creating a fracture plane. However, entanglements limit cavity growth and the density stabilizes at a minimum value. Further wall displacements lead to crazing of adjacent material. The later density profiles (solid lines) show a central crazed region with a well-defined density and uncrazed regions of high density near each wall. From the ratio of these densities we determine $\lambda = 7 \pm 1$. The lower bound comes from the first flat region in the density. This region continues to stretch slightly as the flat region grows, causing the effective value of λ to rise. In the late stages of craze growth, the density spans values corresponding to λ between 6 and 8.

Figure 8b shows the evolution of the density for the system of Figure 6 where $r_c = 1.5\sigma$. The same trends are observed as for $r_c = 2.2\sigma$. The main difference is that the density fluctuations in the crazed region are smaller because the system size is larger. The ratio of the densities again gives $\lambda = 7 \pm 1$. Thus, we see no significant shift in λ with r_c, even though D_0 and S change substantially. Moreover, the value of λ is consistent with eq 3.1 and previous estimates of N_e.

D. Bond Length Distributions. As noted in section IIA, one of the artificial features of the bead−spring model is that bonds are not allowed to break. To determine whether chain scission would be likely if a more realistic potential were used, we monitor the distribution of bond lengths within the polymers. This in turn allows us to find the distribution of bond energies and forces.

Figure 9 shows the logarithm of the probability $P(r)$ that a bond has length r for (a) $r_c = 2.2\sigma$ and (b) $r_c = 1.5\sigma$. The equilibrium distributions for $T = 0.3\epsilon/k_B$ are sharply peaked functions (dashed lines). The maximum probability is shifted inward slightly from the minimum in the nearest-neighbor potential (0.961σ) due to the attractions to more distant beads.

The tensile forces imposed during craze thickening lead to an increase in the number of stretched bonds. The main effect on the probability is to increase the tail in the distribution at large r. The apparent slope of log $P(r)$ gradually becomes less negative as more of the polymers become part of the craze. This development is illustrated in (a) where we show the distribution for times corresponding to the last two panels of Figure 4 (solid line) and for slightly larger times (dash−dotted line) where the distribution is widest. In (b), only the final stage of craze formation is shown.

One way of measuring the magnitude of the change in the distribution function is to determine an effective increase in temperature that would yield a comparable increase in the probability of large r bonds. The dotted lines in Figure 9 show the equilibrium distribution for $T = 0.8\epsilon/k_B$, which is above the glass transition but well below the temperature of $1.1\epsilon/k_B$ used in studies of reptation with the bead−spring model. The large r tail of this equilibrium distribution coincides with the tail for late stages of craze formation with $r_c = 2.2\sigma$. The distribution for $r_c = 1.5\sigma$ is much narrower, which is not surprising given the smaller stresses observed in this system.

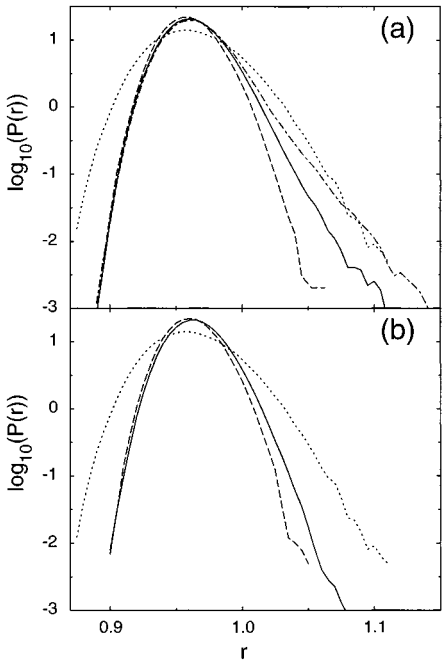

Figure 9. Probability that a bond has a given length r as a function of r for (a) $r_c = 2.2\sigma$ and (b) $r_c = 1.5\sigma$. The equilibrium distributions of bond lengths are shown for $T = 0.3\epsilon/k_B$ (dashed line) and $0.8\epsilon/k_B$ (dotted line). The solid lines show the distribution for a well-developed craze. In (a) these data come from between the last two snapshots in Figure 4. The dashed−dotted line in (a) shows an even later stage when the craze is being stretched prior to failure at the top wall.

The distribution functions in Figure 9 are not sensitive to extreme tails in the probability. These were studied by gathering statistics on all bonds that exceed $r = 1.2\sigma$ during the course of each simulation. For simulations with $r_c = 1.5\sigma$, no bond ever exceeded this length during craze thickening (although some did during equilibration at elevated temperatures). For simulations with $r_c = 2.2\sigma$, long bonds were only observed during the late stages of rupture. For example, in Figure 4, no bonds exceeded 1.2σ until after the fourth snapshot shown. In subsequent growth, there are two bonds that become highly stretched. The maximum length of these bonds fluctuates to 1.25σ by the second to last snapshot in Figure 4 and to 1.29σ by the final snapshot. Both lengths then rise briefly, reaching maxima of 1.30σ and 1.35σ, respectively, but only for a single time step.

To estimate whether such lengths would lead to chain scission, we note that the carbon−carbon bonds along the backbone of a typical polymer are much stronger than the nonspecific van der Waals interactions between polymers. Typical binding energies are 360 kJ/mol or 3.6 eV for carbon−carbon bonds, while values of ϵ are about 100 times smaller.[17] The ratio between the forces needed to break the two types of bonds is even larger, since the energy of the short carbon−carbon bonds changes more rapidly with distance. The magnitude of the maximum attractive force for the Lennard-Jones potential is $f_m^{LJ} = 2.4\epsilon/\sigma$. This corresponds to ∼0.02 nN, using typical values of $\epsilon = 3$ kJ/mol and $\sigma = 0.5$ nm. Odell and Keller[30] have estimated the force f_s needed to break chains using elongational flow experiments and find $f_s = 2.5-12$ nN. Kausch[31] has arrived at the similar estimate of $f_s = 3$ nN. We thus conclude that chains will not break until the force is more than 100 times larger than f_m^{LJ}.

For the bead−spring model the ratio of the force to f_m^{LJ} reaches 50 at a separation of 1.243σ, 100 at 1.365σ, and 150 at 1.41σ. At most four bonds (out of 10^5) ever experienced forces greater than $50f_m^{LJ}$ in any of our simulations with $r_c = 2.2\sigma$, and no bonds experienced forces above $100f_m^{LJ}$. Thus, adding a realistic criterion for chain scission to our potential would have had no effect on our simulations. Even if f_s was as small as $50f_m^{LJ}$, scission would have occurred in the very late stages of growth after the fibril structure and spacing had been determined.

Note that two factors could make scission more likely in experimental crazes. The first is that the crazed region is placed under an increasing tension as the crack tip approaches (Figure 1). This increases the stress above the plateau value and stretches all the bonds. Brown[6] has discussed this process and concluded that the ultimate toughness of crazes is related to their elastic properties and the value of f_s needed to break chains in the expanded craze. The second is that the potential used between nearest-neighbor beads (eq 2.2) is not realistic at the large separations reached before scission occurs. It is concave up for all separations and varies more slowly with r than more accurate potentials. Future simulations will be needed to determine the effect of the potential on bond scission.

IV. Summary and Conclusions

We have examined the rupture of glassy polymers under tensile loading as the chain length N increases. The initial phases of rupture are the same for all chain lengths. The stress rises to a maximum and then drops as cavities nucleate in the polymer. If $N < N_e$, these cavities merge to form a fracture plane, and the toughness is only a few times the lower bound of 2γ. If the chains are entangled ($N > N_e$), deformation around the initial cavities is arrested when the density has dropped by a factor of λ. At this point the region around the initial cavities is strain-hardened and no longer expands. Instead, adjacent material in a narrow active zone is deformed to become part of a growing fibril network. The stress remains fixed at a plateau value S during craze growth. Our simulations give values of S that are of order 20−50 MPa, which is comparable to experimental values. Many models[3,4,8] assume that S equals the capillary pressure at the tips of the expanding cavities between fibrils (Figure 5). However, our calculated values are consistently larger than this.

In our simulations, crazing continues until the entire volume of the polymer is deformed. Then the polymer pulls free from one wall. The value of G is limited only by the system size, and $G/2\gamma$ reached 300 in our largest systems. Experiments show that craze growth is eventually stopped by new mechanisms at micrometer scales.[6] This will be an interesting topic for future simulations, although it will be difficult to simulate such large scales directly.

The simplest view of the role of entanglements is that they act like unbreakable chemical cross-links. One can then derive the estimate for λ_{max} given in eq 3.1.[4] Our observed value of $\lambda = 7 \pm 1$ is consistent with the range $\lambda_{max} = 6 \pm 1$ predicted from eq 3.1 and previous estimates[17,18] of N_e. This extension ratio is somewhat larger than that observed in most experimental systems because our model polymers are unusually flexible.

The structure of our simulated crazes resembles those observed in experiments. Polymers are bundled into highly aligned fibrils that merge and split to form a complex network. The fibril diameter D and spacing D_0 decrease with the surface tension, which was varied by changing the interaction potential. This surface tension dependence is roughly consistent with predictions by Kramer et al.[3,4] Krupenkin and Fredrickson[8] predicted no dependence on γ, but part of our observed change could be due to changes in T_g and the presence of lateral stresses. Our measured spacing for the more realistic choice of potential ($r_c = 2.2\sigma$) corresponds to about 20 nm. This is comparable to typical experimental values, e.g., 30 nm for polystyrene.[4]

The level of agreement between our simulations of craze thickening and previous experimental data indicates that future, more detailed analysis may provide a molecular level understanding of how and why crazes form. One of the unanswered questions is when the crazing zone increases through deformation of new uncrazed material and when it simply expands because fibrils extend and thin. In our simulations, as well as in experiments, the first mechanism predominates. The precise way in which entanglements inhibit fibril thinning has yet to be explored. Other issues concern the role of surface tension: How much of the toughness and plateau stress can be attributed to the interface, and how much comes from deformation and stress within the fibrils? These are some of the issues currently being investigated.

Acknowledgment. We thank S. Barsky, D. Gersappe, E. Kramer, and T. N. Krupenkin for useful discussions and J. Rottler for providing values of γ and detailed comments on the manuscript. Support from the Semiconductor Research Corporation and National Science Foundation Grants 9634131 and 0083286 is gratefully acknowledged.

References and Notes

(1) Pocius, A. V. *Adhesion and Adhesive Technology: An Introduction*; Hanser: Munich, 1997.
(2) Wool, R. P. *Polymer Interfaces: Structure and Strength*; Hanser: Munich, 1995.
(3) Kramer, E. J. *Adv. Polym. Sci.* **1983**, *52*, 1.
(4) Kramer, E. J.; Berger, L. L. *Adv. Polym. Sci.* **1990**, *91*, 1.
(5) Döll, W. *Adv. Polym. Sci.* **1983**, *52*, 105.
(6) Brown, H. R. *Macromolecules* **1991**, *24*, 2752.
(7) Krupenkin, T. N.; Fredrickson, G. H. *Macromolecules* **1999**, *32*, 5029.
(8) Krupenkin, T. N.; Fredrickson, G. H. *Macromolecules* **1999**, *32*, 5036.
(9) Baljon, A. R. C.; Robbins, M. O. *Science* **1996**, *271*, 482.
(10) Baljon, A. R. C.; Robbins, M. O. *Mater. Res. Soc. Bull.* **1997**, *22*(1), 22.
(11) Gersappe, D.; Robbins, M. O. *Europhys. Lett.* **1999**, *48*, 150.
(12) Baljon, A. R. C.; Robbins, M. O. *Theor. Comput. Polym. Sci.* **1999**, *9*, 35.
(13) Mott, P.; Argon, A.; Suter, U. *Philos. Mag.* **1993**, *68*, 537.
(14) Mott, P.; Argon, A.; Suter, U. *Philos. Mag.* **1993**, *67*, 931.
(15) Stevens, M. J. *Macromolecules* **2001**, *34*, 2710, to be published.
(16) Michler, G. H. *Colloid Polym. Sci.* **1986**, *264*, 522.
(17) Kremer, K.; Grest, G. S. *J. Chem. Phys.* **1990**, *92*, 5057.
(18) Pütz, M.; Kremer, K.; Grest, G. S. *Europhys. Lett.* **2000**, *49*, 735.
(19) Thompson, P. A.; Robbins, M. O. *Phys. Rev. A* **1990**, *41*, 6830.
(20) Allen, M. P.; Tildesley, D. J. *Computer Simulation of Liquids*; Clarendon Press: Oxford, 1987.
(21) Grest, G. S.; Kremer, K. *Phys. Rev. A* **1986**, *33*, 3628.
(22) Hoover, W. G. *Annu. Rev. Phys. Chem.* **1983**, *34*, 103.

(23) Doi, M.; Edwards, S. F. *The Theory of Polymer Dynamics*; Clarendon Press: Oxford, 1986.
(24) Fetters, L. J.; Lohse, D. J.; Richter, D.; Witten, T. A.; Zirkel, A. *Macromolecules* **1994**, *27*, 4639.
(25) Bennemann, C.; Paul, W.; Binder, K.; Dünweg, B. *Phys. Rev. E* **1998**, *57*, 843 gives $T_g = 0.45\epsilon/k_B$ for $N = 10$ and a pressure of 1 $\epsilon\sigma^{-3}$. Results for longer chains at zero pressure[9,10] indicate $T_g \approx 0.5\epsilon/k_B$.
(26) Rottler, J.; Robbins, M. O., unpublished.
(27) Brown, H. R.; Kramer, E. J. *J. Macromol. Sci., Phys.* **1981**, *B19*, 487.
(28) Brown, H. R. *J. Polym. Sci., Polym. Phys.* **1983**, *21*, 483.
(29) Layering produces density oscillations near the walls. These are not of interest here, and the binning has been chosen to minimize their influence on the curves.
(30) Odell, J. A.; Keller, A. *J. Polym. Sci., Polym Phys. Ed.* **1986**, *24*, 1889.
(31) Kausch, H. H. *Polymer Fracture*, 2nd ed.; Springer-Verlag: Berlin, 1987.

MA0012393